Arsenic removal procedure for the electrolyte from a hydro-pyrometallurgical complex

D.C. Paz-Gómez[a,*], S.M. Pérez-Moreno[a], M.J. Gázquez[b], J.L. Guerrero[a], I. Ruiz-Oria[c], G. Ríos[c], and J.P. Bolívar[a]

[a]Department of Integrated Sciences, Research Centre on Natural Resources, Health and the Environment (RENSMA), University of Huelva, 21007, Huelva, Spain

[b]Department of Applied Physics, Marine Research Institute (INMAR), University of Cadiz, 11510, Cádiz, Spain

[c]Atlantic Copper S.L.U., 21001, Huelva, Spain

*Corresponding author: E-mail address: manuel.gazquez@dfa.uhu.es; Phone number: +34 956 01 6935; Postal address: Department of Applied Physics, Marine Research Institute (INMAR), University of Cadiz, 11510, Cádiz, Spain

Abstract

Commercial copper (Cu) is obtained by a hydro-pyrometallurgical process, where the Cu anodes obtained in the furnaces (Cu > 99.5%) are enriched up to 99.99% in "cathodes" by electrorefining at an electrolysis plant. During this process, some impurities accumulate in the electrolyte, mainly arsenic (As), which decrease the quality of the Cu cathode. For this reason, the electrolyte is sent to an electrolyte cleaning plant (ECP) for its purification. Electrolyte sludge (ES) is produced in the last stage of purification and is recirculated back to the furnace due to the high Cu content. This recirculation involves a severe problem of As accumulation in the industrial process. The objective of this work was to develop a procedure to fully dissolve the ES, removing the As and recovering its Cu content. The ES dissolution process was optimised (dissolution efficiency > 99%) in H_2SO_4 (1.4 M)/HNO_3 (1.8 M) medium using a 1:20 g mL^{-1} solid-to-liquid ratio. As was removed from the ES solution by its precipitation as iron (III) arsenate, with high efficiency (more than 70%). After As removal, the Cu can be precipitated as copper sulphate, which is used in several applications.

Keywords: Electrolyte sludge; Ferric arsenate; Scorodite; Arsenic removal; Copper–arsenic solution

1. Introduction

The demand for copper (Cu) minerals has increased quickly over the last 50 years, and it is expected to keep growing due to the essential role of Cu in modern technologies. Worldwide refined Cu production reached 24 Mt in 2019, and it involves a large amount of waste and wastewater generation (ICSG, 2020). In recent decades, the manufacturing industry has tried to develop policies to reduce the environmental impact and to achieve sustained economic growth, following the current strategic lines aimed at ensuring the implementation and development of the "Circular Economy" through the efficient use of raw materials and residues. Therefore, policies on waste management must be directed apply the hierarchy established by normative: prevention, reduction, reuse, and recycle. A proper waste valorisation represents an excellent management alternative producing economic and environmental benefits. For this, industries have introduced effective resource management consisting of recycling, reusing, and valorisation of these ones,

reducing the production cost and decreasing risks for the environment and human health (Khan et al., 2021, 2020; Liao et al., 2019).

Atlantic Copper S.L.U, located in Huelva (Spain), is one of the biggest manufacturers of ultrapure Cu cathodes (> 99.99% Cu) in Europe, producing more than $3 \cdot 10^5$ t y^{-1} (Atlantic Copper, 2017). During Cu electrorefining, the concentrations of the raw material impurities, such as As, Sb, Bi, Ni, etc., gradually increase in the electrolyte, which negatively affects the quality of the Cu cathode; therefore, the impurities must be removed. For this, a fraction of the electrolyte is continuously sent to an electrolyte cleaning plant (ECP) to reduce the level of impurities, especially As, and to recover a significant fraction of the Cu that is not electrodeposited in the cathode ("decopperising").

The electrolyte cleaning process involves three stages by electrowinning in liberator cells (Artzer et al., 2018; Wesstrom and Araujo, 2012). Firstly, the Cu concentration is reduced from 45 g L^{-1} to 25 g L^{-1}, providing a B-grade Cu cathode (> 99.97% Cu), which is commercialised. Secondly, the Cu concentration is further reduced to around 10 g L^{-1}. Finally, in the third step, the remaining Cu, and most of the As, is removed from the solution in the electrolyte sludge (ES). In the Huelva factory, about 1300 t of ES are produced annually. The final treated electrolyte is returned to the electrolyte tank for reuse.

Currently, the ES is sent to a flash smelting furnace (FSF) to recover its Cu content (≈ 60%), but this causes the accumulation of As during the industrial process, generating problems during liquid effluent treatment. Fig. 1 shows the procedure developed in this work for As-free Cu recovery, which consists of dissolving the ES by acid digestion, and then the As removal from the obtained dissolution (ES wastewater) by precipitation with iron as ferric arsenate. Finally, the As-free solution may be used in two different ways: Cu is recovered as copper (II) sulphate pentahydrate ($CuSO_4 \cdot 5H_2O$) and returned to the industrial process or it is valorised in commercial applications, such as agriculture. On the other hand, the resulting industrial wastewater stream, with low pollutant content, can be sent to an effluent treatment plant (ETP) for final treatment before it is released into the environment. The novelty of the proposed procedure is the combination of different chemical processes (digestion, precipitation, and crystallisation) applied to the ES to achieve As removal and Cu recovery. Currently, this waste is a recirculating waste of the Cu metallurgy process, of which no treatment is known for the separation of both elements.

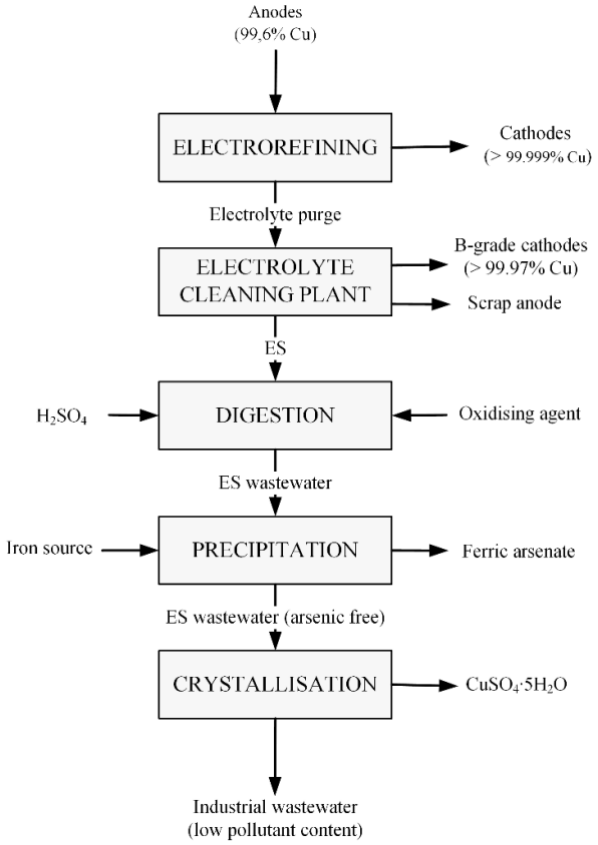

***Fig. 1**. Flowchart of the electrolyte sludge (ES) and the proposed treatment.*

There have been no previous studies describing As removal from ES. Most research has been focused on other co-products, such as slag, dust, or anode slime (Demopoulos, 2014; Min et al., 2015; Schwartz et al., 2017). In addition, there have been some investigations of As removal from waters for human consumption and/or industrial wastewater (Jain and Singh, 2012; Litter et al., 2010), and the methods used to reduce the As concentration in the solutions were precipitation, adsorption (Cao et al., 2021; Chen et al., 2015; Hao et al., 2018), the use of ion exchange resins (Balaji et al., 2005; Lenoble et al., 2004), and the use of newly developed methods, such as electrocoagulation or membrane treatment (Nidheesh and Singh, 2017; Song et al., 2017; Zouboulis and Katsoyiannis, 2018). Nevertheless, the United States Environmental Protection Agency (EPA) designated As removal by co-precipitation with ferric ions in a liquid effluent as “the best demonstrated available technology (BDAT)” for As disposal (Rosengrant and Fargo, 1990). For that reason, this method has been the most researched in the last decades (Demopoulos, 2014; Fujita et al., 2008a; Le Berre et al., 2007; Schwartz et al., 2017; Zhang et al., 2019). The precipitation reaction can be expressed as the following:

$$4H_3AsO_{4(aq)} + 4FeSO_{4(aq)} + O_{2(g)} + 6H_2O_{(aq)} \leftrightarrow 4FeAsO_4 \cdot 2H_2O_{(s)} + 4H_2SO_{4\ (aq)} \quad \textbf{Eq. 1}$$

Considering the above facts, the central objective of this study was to remove the As from the dissolution of ES coming from the ECP, generating a final solution more suitable for recovering the dissolved copper sulphate. Firstly, ES dissolution tests were carried out. Then, the removal of As by precipitation with Fe was studied. The final solutions were analysed using various analytical techniques to determine the precipitation efficiency (PE) of the main elements, especially As and Cu, and the physical–chemical characteristics of the formed solids were studied.

2. Materials and methods

2.1. Materials

The ES employed in this research was collected from Atlantic Copper S.L.U in 2017. Six sampling campaigns were organised (one per week) with the aim of analysing the possible temporal variability in the characteristics of the ES. After collection, the samples were dried at 60 ºC to constant weight.

All iron reagents [$FeCl_3$, $Fe_2(SO_4)_3 \cdot 7H_2O$, $FeSO_4 \cdot 7H_2O$], arsenic reagent [$As_2O_5 \cdot 3H_2O$] and alkaline agents [$Ca(OH)_2$ and $Mg(OH)_2$] employed in this work were of analytical grade (purity > 95%) and from Merck Company. The concentrations of the acids used were the following: 96% H_2SO_4 and 65% HNO_3. In addition, the oxygen used had a purity of > 99.5%.

2.2. Experiments

2.2.1. Dissolution of the electrolyte sludge (ES)

The dissolution of the ES was performed in acid medium by using sulphuric acid (H_2SO_4). The influence of temperature, the solid-to-liquid ratio, and the type of oxidising agents (air, oxygen and HNO_3) were studied. Firstly, the dissolution of ES was done applying a mixture of sulphuric acid (H_2SO_4) and nitric acid (HNO_3) solution, in which the solid-to-liquid ratio, molar concentration, temperature and reaction time, were changed and then the influence of using other oxidising agents (air and oxygen) was investigated.

The ES dissolution experiments with H_2SO_4 and HNO_3 were carried out in an uncovered reaction vessel with a volume of 1 L (see Fig. S1a). These experiments simulated different conditions: 1) solid-to-liquid

ratios of 1:10 and 1:20 g mL^{-1} were used; 2) the H_2SO_4 and HNO_3 concentrations used ranged from 0.9 to 2.7 M and from 1.0 to 1.8 M, respectively; 3) the temperature and reaction time were 24, 50, and 80 ºC and 12 and 2.5 h, respectively. A summary of these experiments is shown in Table S1 of the supplementary material, to note that the experiments with a solid-to-liquid ratio of 1:10 g mL^{-1} were not included in this table because the results obtained were not relevant. The solution was continuously agitated with a magnetic stirrer (500 rpm). Finally, the experimental solution was filtered to separate the obtained phases. The solid was rinsed with water and dried until a constant weight was obtained.

The experiments with air or O_2 were carried out in a 1 L reaction vessel (1 L beaker) covered with a lid with holes through which a thermocouple and air/O_2 channels were introduced (2 L min^{-1} and 8 L min^{-1}, respectively) (see Fig. S1b). In the experiment with air, different concentrations (2, 4, 6, and 10 M) of a H_2SO_4 solution were used (see Table S1). When O_2 was used, the experiment was performed with a 2 M H_2SO_4 solution. In both experiments, the solution was heated to 80 ºC and continuously agitated with a magnetic stirrer at 500 rpm. Finally, the solution was filtered to separate the solid from the liquid phase. The solid phase was rinsed with water and dried at 60 ºC to constant weight.

The tests were codified as "X-Y-Z-W-R", where "X" is the oxidising agent used to dissolve the sludge (N is nitric acid, O is oxygen, and A is air), "Y" represents the concentration of HNO_3 (M) or the gas flow of air or oxygen (in L min^{-1}), "Z" is the concentration of H_2SO_4 used, "W" is the time (h) and temperature (ºC) of the experiment (where A is 12 h and 24 ºC, B is 2.5 h and 50 ºC, and C is 2.5 h and 80 ºC), and "R" indicates if the sample was a replica. For example, N-1.6-1.8-A is a sample with HNO_3 as the oxidising agent (1.6 M) and the use of 1.8 M of H_2SO_4, with an experimental time of 12 h at 24 ºC, and A-2-4-C-R is a sample using air as the oxidising agent (2 L min^{-1}) and 4 M of H_2SO_4, with an experimental time of 2.5 h at 80 ºC, and it is a replicated sample.

2.2.2. Arsenic removal

To study the elimination of As, two solutions were used for the experiments. One solution, named the artificial solution, contained 10 g L^{-1} of the As prepared in the laboratory using arsenic (V) oxide hydrate [$As_2O_5 \cdot 3H_2O$], and the second solution was obtained by fully dissolving the ES. In Table S2 of the supplementary material, a summary of the experimental conditions for As removal is shown.

The experiments for As precipitation were carried out in three stages by gradually increasing the pH since protons are released during the formation of $FeAsO_4 \cdot 2H_2O$, which then decreases the pH and inhibits scorodite formation (see Eq. 1).The precipitation of $FeAsO_4 \cdot 2H_2O$ occurs at a pH of between 1.5 and 3.0, according to the literature consulted.(Droppert et al., 1996; Fujita et al., 2009a). In stage I, the Fe source was added, and the reaction proceeded for 3 h. The As precipitation reaction reaches equilibrium at a final pH that is lower than the initial pH. To favour the precipitation of As, the equilibrium (Eq. 1) should be moved to the right by decreasing the acidity (stage II). This is achieved by adding an alkaline agent up to a pH around 2.5, reaching newly the equilibrium (pH ≈ 1.5) after around 3 h. Then, the pH is increased to around 3 by another alkali addition (stage III), reaching a final pH of around 2 after equilibrium.

Arsenic removal using an artificial solution

Experiments with artificial solution focused on looking for the most suitable method for the synthesis of $FeAsO_4 \cdot 2H_2O$. In experiment E1-A, As removal with two compounds as Fe^{3+} sources [$FeCl_3$ and $Fe_2(SO_4)_3 \cdot 7H_2O$] and a As/Fe molar ratio of 1.5 without pH adjustment was carried out. The As precipitation experiments were done under continuous stirring (400 rpm) at 85 ºC for 6 h. In experiment E1-B, $FeSO_4 \cdot 7H_2O$ was employed as the Fe^{2+} source. In this experiment, air was injected at a rate of 1–2 L min^{-1} to oxidise the Fe^{2+} into Fe^{3+} under similar experimental conditions as experiment E1-A.

In experiments E2 and E3, the precipitation was performed through three stages of pH adjustment using $Ca(OH)_2$ or $Mg(OH)_2$, respectively. Ferrous sulphate was used in both experiments as the Fe source, with air used as the oxidising agent. The experimental conditions were the same as those used in experiment E1-B, except the reaction time that in E2 and E3 was 3 h for each stage. In stage I, pH adjustment was not necessary because the solution pH was around 1.5, but in stages II and III, the pH was adjusted to around 2 and 2.5, respectively. These experimental conditions are summarised in Table S2 of the supplementary material. The equipment used in the As removal experiments consisted of an air pump, a flowmeter, a mechanical stirrer, a heating plate with temperature control, a beaker with a lid used as the reaction vessel, and a thermal jacket.

Arsenic removal from the ES solution

Experiments E4 and E5 for As removal were carried out in three stages of pH adjustment using $Ca(OH)_2$ and $Mg(OH)_2$ as alkali reagents, respectively, following the same methodology of previous experiments (E2 and E3) (see Table S2). However, in both experiments, an initial stage was performed in which the pH was increased from an initial value of less than 0.5 (pH of the ES solution) to 1.5 to achieve the ferric arsenate precipitation (Droppert et al., 1996; Fujita et al., 2009a).

2.3. Analytical techniques of characterisation

The solids obtained from both ES dissolution and As removal experiments were subjected to different analytical techniques for their physicochemical characterisation. 1) X-ray fluorescence (XRF) (Panalytical sequential spectrometer, AXIOS model) was used to determine the major elements. 2) X-ray diffraction (XRD) with a Panalytical X'Pert Pro diffractometer and X'Pert HighScore Plus software was used to identify the mineral phases. 3) Thermogravimetric analysis (TGA) and differential scanning calorimetry (DSC) were used to study the thermal behaviour of the samples using a METTLER-TOLEDO TG/DSC2 thermobalance coupled to an inductively coupled plasma mass spectrometer (ICP-MS) (NETZSCH QMS-403 Aëolos Quadro) to determine the composition of the residual gases. 4) Scanning electron microscopy (SEM) (QUANTA-Fei 200) equipped with an energy dispersive spectrometer (EDS) was employed to study the morphology and microstructure of the solids. 5) The trace elements were analysed by ICP-MS (Perkin Elmer Sciex ELAN 9000) and inductively coupled plasma optical emission spectroscopy (ICP-OES) (Varian 735-ES) in the Activation Laboratories (Actlabs) from Canada, accredited in the norm ISO/IEC 17025:2017.

To ensure the repeatability of the experiments, two replicates of each were performed. When required, quality control (QC) of the analytical techniques was performed by measuring several certified reference materials (CRMs), duplicates, and blanks.

3. Results and discussion

3.1. ES dissolution

The ES sample used in the experiments contained a high Cu concentration (54±1%), but it also had As (10±1%) and S (7±1%) in minor proportions. Copper was present mainly as Cu metal (Cu) and cuprite (Cu_2O). In addition, another significant Cu fraction was associated with As, forming domeykite (Cu_3As).

189 The S content was also associated with Cu as poitevinite ($CuSO_4 \cdot H_2O$), see Fig. 2. Other elements, such as
190 Bi, Fe, Ni, Pb, Sb, and Zn, were found at concentrations below 1%.

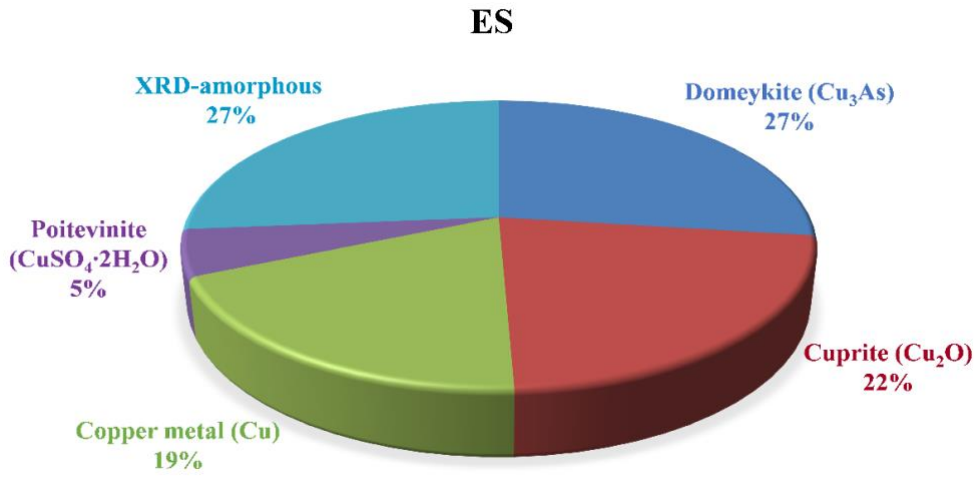

Fig. 2. *Mineral phases of the ES.*

191

192 The dissolution percentage of the components present in the ES, focusing on Cu and As, was studied
193 through several experiments described in the materials and methods section. The results are presented in
194 Fig. 3. In addition, the chemical composition of the obtained solution can be seen in Fig. S2 of
195 supplementary material.
196 Similar results were obtained in the starting batch experiments and their replicates; therefore, only one of
197 them are shown in Fig. 3a. The ES was not completely dissolved when air or O_2 was used (A-2-2-C and O-
198 8-2-C, respectively). The dissolution efficiency, in mass, of the whole ES sample in these experiments was
199 32% and 65%, respectively, when 2 M H_2SO_4 was used. By using air, the Cu and As dissolved fractions
200 were about 30% and 5%, respectively, while about 75% of Cu and 33% of As was reached with oxygen.
201 The dissolution efficiency for the rest of the elements depends on the chemical solubility of each metal.
202 For example, about 60% of Ni was dissolved in both experiments. To point out that S was fully dissolved
203 in the three experiments (see Fig. 3a), and this can be explained by considering that S is in the ES as
204 poitevinite ($CuSO_4 \cdot H_2O$), see Fig. 3b.
205 On the contrary, the ES was fully dissolved in a solution of 1.4 M H_2SO_4 and 1.8 M HNO_3 for 2.5 h at 50
206 ºC (N-1.8-1.4-B) (see Table S1 of the supplementary material), achieving a dissolution efficiency of the

ES of around 99.95%. Fig. 3a shows that the dissolution efficiency of almost all major elements was about 100%, while the dissolution efficiency of Ni was around 80%. Therefore, this dissolution method was employed to obtain the ES solution used in the As removal experiments. The ES solution obtained in experiment N-1.8-1.4-B was mainly composed of S (≈ 46 g L^{-1}), Cu (≈ 36 g L^{-1}), and As (≈ 5.2 g L^{-1}). Furthermore, the solutions presented concentrations of Bi, Sb, Ni, and P (100–250 ppm) and Fe, Pb, Te, and Zn (< 20 ppm) as trace elements (see Fig. S2 of the supplementary material).

To analyse the relationship between the elements with higher concentrations and the undissolved minerals from the ES, the mineralogy of the ES and the obtained final solids after acid attack was determined by XRD. In Fig. 3c, the proportion of undissolved mineral phases for A-2-2-C and O-8-2-C is shown. In experiment A-2-2-C, the dissolution of cuprite, copper metal, and domeykite was around 23%, 63%, and less than 1%, respectively, whereas in O-8-2-C, more than 90% of Cu_2O and Cu and around 80% of Cu_3As were dissolved. In both experiments, $CuSO_4 \cdot H_2O$ was completely dissolved.

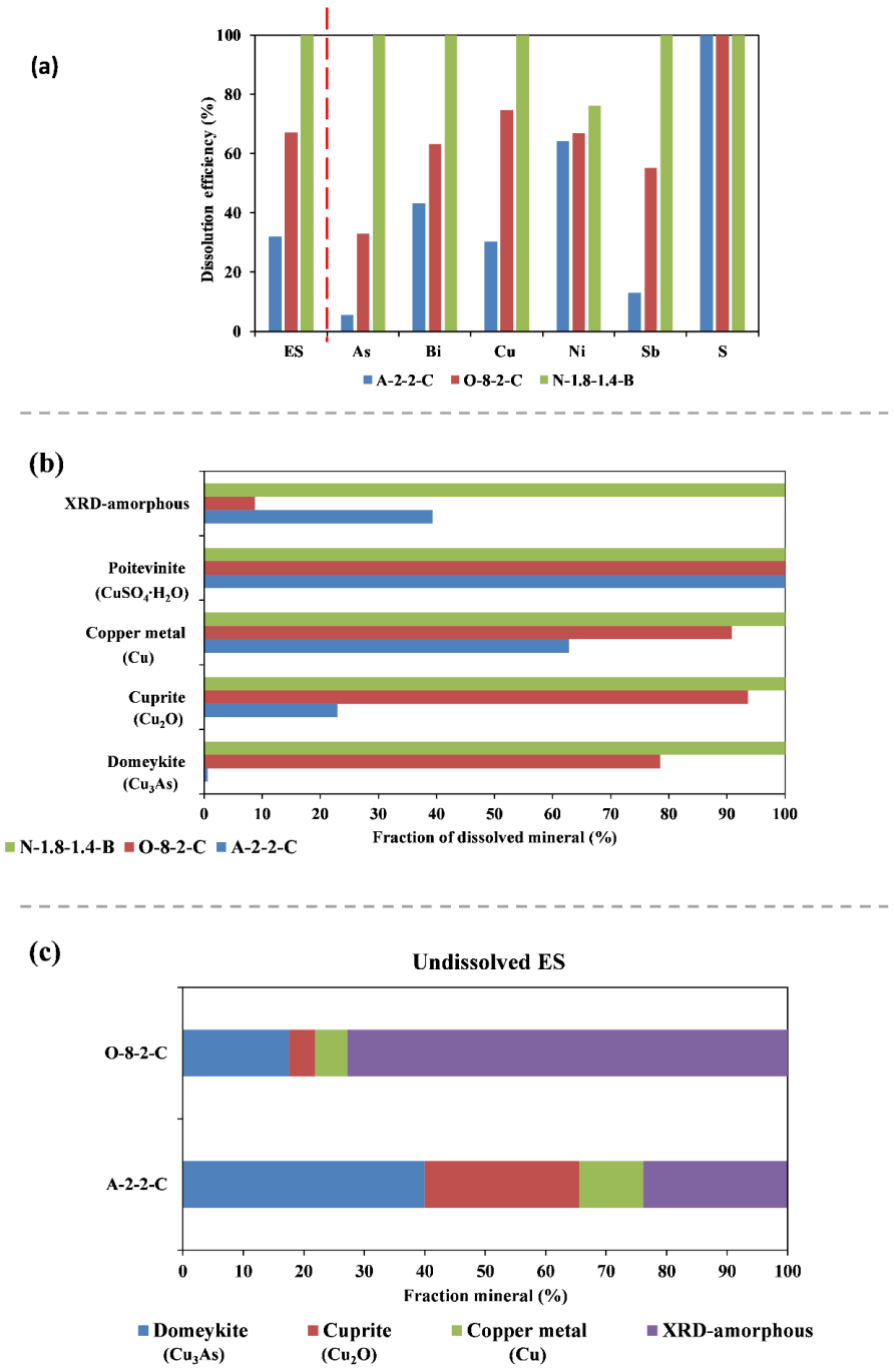

Fig. 3. *Dissolution efficiency (%) of the major elements contained in the ES matrix by using different dissolution methods. (a). Fraction of dissolved mineral (%) in the experiments (b). Mineral phases presented in the undissolved ES (c).*

219

220 **3.2. Time evolution of the experiments**

221 The evolution of the experiments over time was evaluated by measuring the pH and oxidation–reduction

222 potentials (ORPs). Fig. 4a shows the evolution of pH versus time, while Fig. 4b presents the correlation

223 between pH and ORPs. In experiments E2 and E5, $Ca(OH)_2$ was used as neutralising to increase the pH,
224 while $Mg(OH)_2$ was added in experiments E3 and E4 (see Table S2).
225 For experiments E3 and E4, the pH decreased in the first 60 min (stage I), and after that no significant
226 changes were observed (Fig. 4a). In stage II, alkali was added until obtaining a pH of around 2.3, and then
227 the pH continuously decreased for 180 min. In stage III, the pH increased to around 2.9, and from this time
228 the same trend as in the previous stages was observed. As can be seen, the pH changes are similar in both
229 solutions when $Mg(OH)_2$ was used as the basic agent (Fig. 4a) since $Mg(OH)_2$ does not interfere with the
230 formation of ferric arsenate (solid).
231 On the other hand, experiments E2 and E5, in which $Ca(OH)_2$ was used to increase the pH, did not show
232 the same patterns as experiments E3 and E4 due to in E2 and E5 experiments, a secondary reaction between
233 Ca and SO_4 ions is produced forming calcium sulphate which precipitates simultaneously with ferric
234 arsenate (Demopoulos, 2014; Zhang et al., 2019). The possible differences in the pH behaviour with time
235 in experiments E2 and E5 are due to the lower sulphate concentration in the used artificial solution in E2.
236 In stage I, pH slowly decreases until the end of the stage in E2, while for E5 pH decreases during 120 min,
237 and then no significant change was observed (see Fig. 4a). For stage II, the pH decreased faster in
238 experiment E5 than in experiment E2. In the last stage of experiment E5, the pH rapidly decreased in the
239 first 120 min, and then no significant changes were observed, while a continuous decrease was observed in
240 experiment E2 (Dabekaussen et al., 2001; Fujita et al., 2009b).
241 A good linear relationship between the ORP and pH was observed (Fig. 4b), as would be expected
242 considering the Nernst equation, which sets up the logarithmic relationships between the ORP and H^+
243 concentration, suggesting a linear correlation between both parameters. This phenomenon was observed
244 during the experiments (Fig. 4b), where the ORP increased with decreasing pH value.

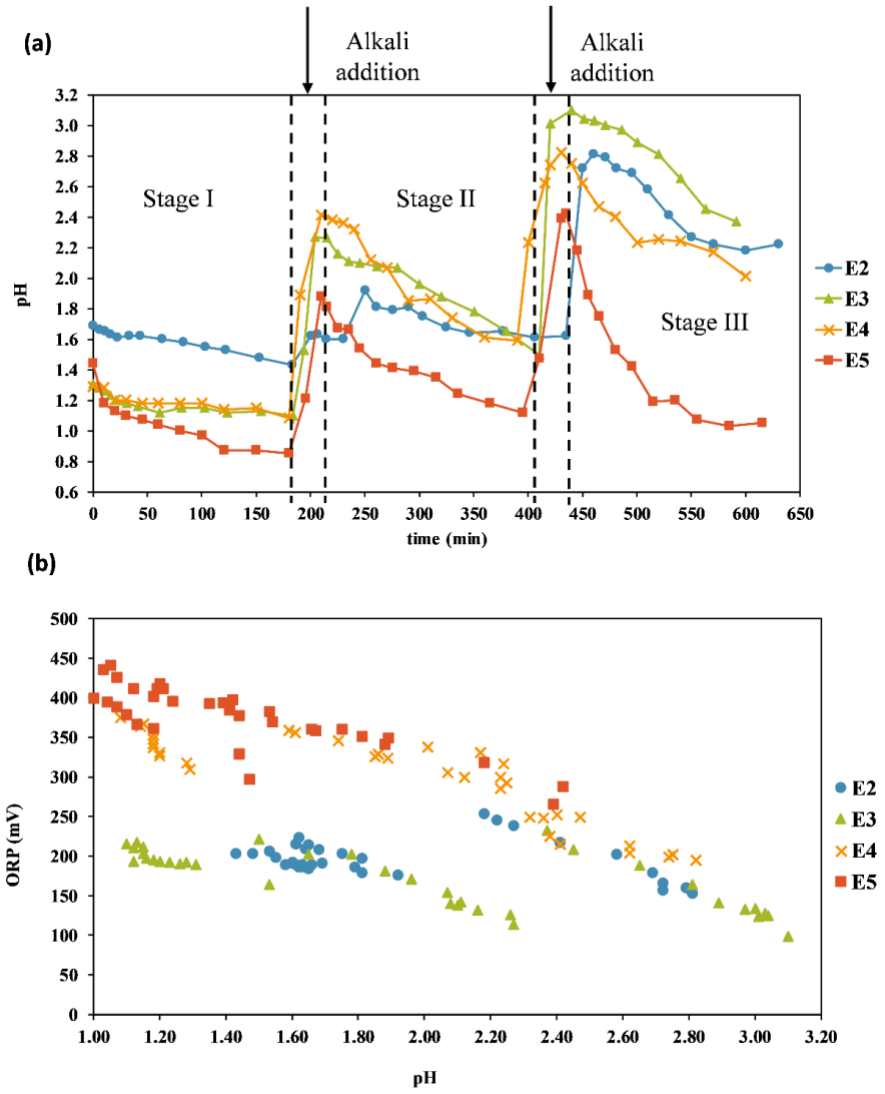

***Fig. 4**. (a) Changes in pH with reaction time and (b) changes in the oxidation–reduction potential (ORP) with the pH of the solution.*

In relation to the change in element concentrations, it is worth noting that Fe and As decreased following the same tendency (Fig. S3), showing that these elements precipitate together. Other major elements such as Cu, Ca, Mg, and S showed different behaviour in each experiment. On the one hand, in experiments E2 and E5, the S concentration decreased due to the addition of $Ca(OH)_2$ since Ca and S precipitate, forming calcium sulphate. On the other hand, in experiment E3, no significant changes were observed in the S concentration, while the concentration of Mg increased, indicating that it does not precipitate (see Fig. S3 of the supplementary material). In experiment E4 (Fig. S3), the Cu, Mg, and S concentrations decreased

with time, suggesting that these elements could co-precipitate. Besides in the experiment E5, the Cu content decreased indicating this could also co-precipitate.

3.3. Precipitation efficiency (PE)

Fig. 5 shows the precipitation efficiency (PE), or the removing efficiency, of the major elements contained in the ES solution as a function of time. It is important to note that this study was not performed in the E1-B experiment (no pH adjustment), but the final As and Fe PEs were calculated, finding that around 65% of As and 35% of Fe were removed from the solution.

In experiments E2 and E5, where $Ca(OH)_2$ was used as an alkaline agent, the PE of As and Fe increased with time, removing up to 99.5% of As and 91% of Fe in experiment E2 (artificial solution), while for experiment E5 (ES solution) the removal of As and Fe was lower, with around 70% removal for both elements. This can be due to the high concentrations of Cu and SO_4 ions in the solution, which probably interfere with and inhibit ferric arsenate formation (Fujita et al., 2008b; Gomez et al., 2011a). The PE of Cu was around 50% in experiment E5, confirming that the Cu co-precipitates with As and Fe, which is a problem for the next Cu recovery stage. Furthermore, the PE for Ca and S in both experiments was higher than 90%, but it is important to note that in experiment E5 before the As removal stages, a pH adjustment was made to 1.5, where Ca and S precipitated as $CaSO_4 \cdot 2H_2O$, resulting in a PE of greater than 80% for both elements.

In experiments E3 and E4, where $Mg(OH)_2$ was used as alkalinising agent, the PE of As and Fe increased over time, similar to the observed trend in experiments E2 and E5, precipitating more than 99.5% of As and 91% Fe in experiment E3 (artificial solution), while the PE of As and Fe in experiment E4 (ES solution) was about 70%. This behaviour is similar to the experiment with $Ca(OH)_2$; therefore, the decrease in PE of both elements is probably due to the high content of Cu and SO_4 ions, which could interfere with ferric arsenate formation (Fujita et al., 2008b; Gomez et al., 2011a). In addition, the PE of S in experiments E3 and E4 was about 50% in both cases, suggesting the co-precipitation of sulphur with the solid $FeAsO_4$.

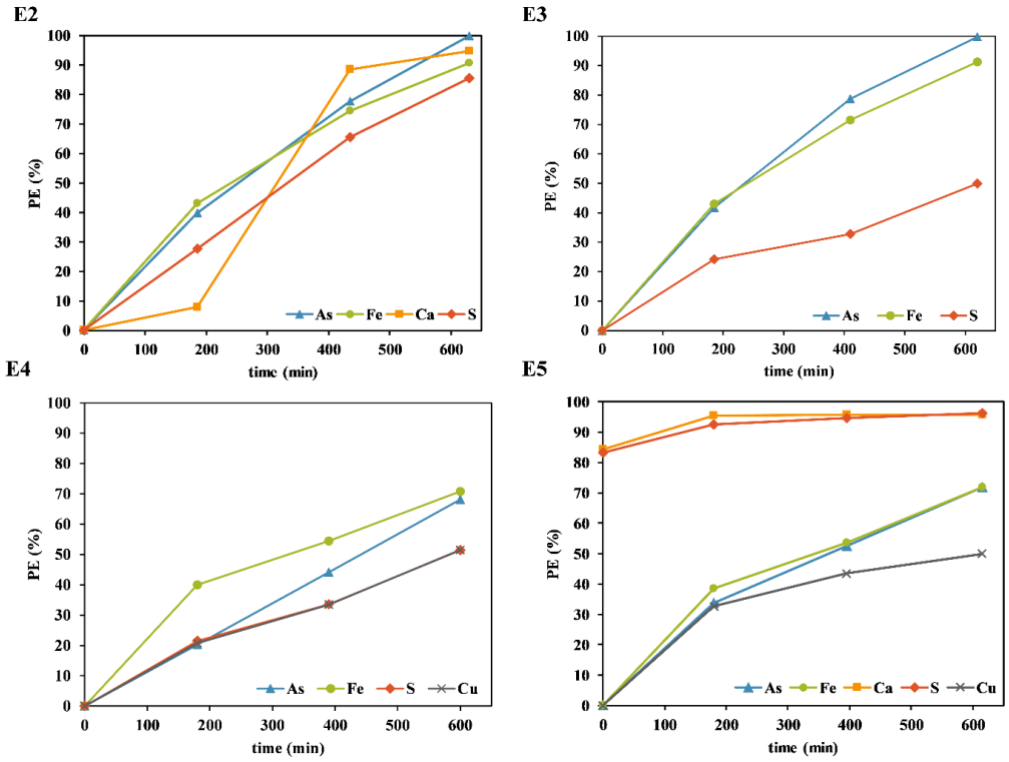

Fig. 5. *Precipitation efficiency (PE) (%) as a function of time for both types of experiments: E2–E3 for the artificial solution and E4–E5 for the ES solution.*

277

278 **3.4. Characterisation of the obtained precipitates**

279 The physicochemical characteristics of the precipitated phases in the As removal experiments using the
280 artificial solution and different Fe^{3+} sources [E1-A1: $FeCl_3$ and E1-A2: $Fe_2(SO_4)_3{\cdot}7H_2O$] are shown in Table
281 S3 of the supplementary material. The solids obtained in these experiments were mainly composed of ≈
282 35% As and ≈ 23% Fe, which is similar to the composition found in $FeAsO_4$, but the diffraction patterns
283 indicated that these solids were in the amorphous form.

284 However, scorodite (≈ 96% $FeAsO_4{\cdot}2H_2O$) was synthesised in experiment E1-B, according to the XRD
285 analysis (Fig. S4 of the supplementary material), where Fe^{2+} was used. The concentrations of the major
286 elements of the obtained solid are presented in Table 1, showing a high concentration of As (39.0±0.1%)
287 and Fe (24.0±0.1%), but also a minor proportion of S (< 0.05%). In addition, the losses on ignition (around
288 14%) agree with the theoretical mass loss (about 15.5%) associated with the loss of the crystallisation water
289 of $FeAsO_4{\cdot}2H_2O$ (Gomez et al., 2011b; Gonzalez-Contreras et al., 2010; Le Berre et al., 2008). The

290 scorodite was probably formed by arsenic precipitation with ferrous ions in the presence of oxygen,
291 following Eq. 1 (Fujita et al., 2008a, 2008c; Min et al., 2015).
292 Furthermore, thermogravimetric analysis was performed to determine the thermal behaviour of the formed
293 scorodite. In Fig. S5 of the supplementary material, 2 thermal events were observed at 220 ºC and 960 ºC.
294 Water was detected in the first event due to the dehydration of scorodite, following Eq. 2 (Gomez et al.,
295 2011b; Gonzalez-Contreras et al., 2010; Le Berre et al., 2007), while O_2 was detected in the second event,
296 suggesting the decomposition of iron arsenate anhydro (Cervando and Viraca, 2013; Cheng et al., 2019),
297 according the chemical Eq. 3.

$$FeAsO_4{\cdot}2H_2O_{(s)} \rightarrow FeAsO_{4(s)} + 2H_2O_{(g)} \qquad \textit{Eq. 2}$$

$$2FeAsO_{4\ (s)} \rightarrow Fe_2O_{3(s)} + As_2O_{3(g)} + O_{2(g)} \qquad \textit{Eq. 3}$$

298 According to the amount of mass lost (15.4%) in the first event, the solid is composed of 99%
299 $FeAsO_4{\cdot}2H_2O$, corresponding to an As concentration of around 32%, which is in line with the results
300 obtained from the XRF and XRD analysis. On the other hand, the mass loss in the second event could not
301 be determined because the event did not finish.
302 Finally, the SEM analysis showed that sample E1-B presents a homogeneous morphology formed by
303 particles mainly composed of As and Fe (point 1 of Fig. S6, supplementary material). Its composition (see
304 table, Fig. S6) and its bipyramidal octahedral structure confirm that these particles are scorodite, with a size
305 of around 20 µm.

	Exp. ID	As	Bi	Ca	Cu	Fe	O	Pb	S	Sb	LOI
Artificial solution	E1-B	39.0 ± 0.1	<DL	<DL	<DL	24.0 ± 0.1	22.9 ± 0.1	<DL	0.03 ± 0.01	<DL	14.2 ± 0.2
	E2	20.8 ± 1.1	<DL	11.0 ± 0.6	<DL	15.0 ± 1.0	32.0 ± 1.0	<DL	10.0 ± 1.0	<DL	10.8 ± 1.1
	E3	36.0 ± 1.9	<DL	<DL	<DL	24.0 ± 0.3	24.0 ± 1.0	<DL	1.0 ± 0.8	<DL	15.1 ± 0.1
ES solution	E4	30.2 ± 1.9	2.7 ± 0.5	<DL	7.7 ± 3.4	22.6 ± 1.4	25.3 ± 0.1	0.16 ± 0.03	2.15 ± 0.01	1.23 ± 0.7	7.8 ± 1.2
	E5	10.9 ± 1.2	0.02 ± 0.01	19.0 ± 0.2	0.6 ± 0.2	10.3 ± 0.1	38.8 ± 0.1	<DL	15.4 ± 0.5	0.12 ± 0.02	4.6 ± 1.7

Table 1*. Average concentrations (%) of the major elements of the formed precipitates in the As removal experiments. LOI=loss on ignition; Detection limit (DL=0.01%). Standard uncertainty (1 σ) was calculated as the standard deviation of the mean,* $\boldsymbol{\sigma = S_x/ (n)^{1/2}}$*, where n=3.*

306

The obtained precipitate of E2 contained As (20.8±1.1%), Fe (15.0±1.0%), Ca (11.0±0.6%), and S (10.0±1.0%) as major elements (Table 1), being gypsum (≈ 50%, $CaSO_4 \cdot 2H_2O$) and scorodite (≈ 36%) the main mineral phases presented (Fig. S4 of the supplementary material). The presence of gypsum was expected when calcium hydroxide was used as a neutralising agent due to the precipitation of calcium sulphate dihydrate as a secondary product (Demopoulos, 2005; Droppert, 1996), according to Eq. 4. The experimental mass ratio (Ca/S = 1.10) was slightly lower than the theoretical value for gypsum (Ca/S = 1.25), according to the consulted literature (Demopoulos, 2005; Dutrizac and Jambor, 2007; Gomez et al., 2011a), this could be due to small incorporation of S (as SO_4) in the structure of the scorodite as a result of $SO_4 \rightarrow AsO_4$ substitution, forming $Fe(AsO_4)_{1-x}(SO_4)_x \cdot 2H_2O$ (Demopoulos, 2005; Dutrizac and Jambor, 2007; Gomez et al., 2011a; Singhania et al., 2005).

$$Ca(OH)_{2(s)} + H_2SO_{4(aq)} \rightarrow CaSO_4 \cdot 2H_2O_{(s)} \qquad \textit{Eq. 4}$$

On the other hand, the proportion of scorodite determined by XRD indicated lower content of As and Fe than that provided by the XRF analysis. This suggests that part of the As and Fe of the sample does not form crystalline scorodite, and therefore that part is associated with the amorphous XRD phase (approximately ≈ 14%) found in this sample.

In Fig. 6, it can be seen that the E2 sample presents a heterogeneous morphology formed by two types of particles: large particles (point 1, Fig. 6) composed of Ca and S, whose tabular crystals correspond to gypsum, and fines particles (point 2, Fig. 6) composed of As and Fe, whose composition and bipyramidal octahedral structure suggest that is scorodite. These results confirm the crystal phases identified by XRD analysis. In addition, the general composition of the E2 sample obtained by EDS analysis showed that this solid is mainly composed of As, Ca, Fe, and S (see table, Fig. 6), which is in line with the XRF analysis.

The E3 sample [pH adjustment with $Mg(OH)_2$] contained As (36.0±1.9%) and Fe (24.0±0.3%) in greater proportions, but it also contained less than 1% of S, which is analogous to the composition of the E1-B sample. In addition, scorodite (≈ 62%) was the only mineral phase identified (see Fig. S4), and this compound is consistent with the obtained loss on ignition (LOI≈15.1%) that is associated with loss of the crystallisation water of $FeAsO_4 \cdot 2H_2O$ (Gomez et al., 2011b; Gonzalez-Contreras et al., 2010; Le Berre et al., 2008). However, the proportion of the mineral phase did not correspond to the composition given by

XRF, meaning that part of As and Fe was found in the amorphous phase (≈38%), which is significantly high compared to that obtained in the E1-B (≈ 4%) and E2 (≈ 14%) samples.

Moreover, the SEM analysis showed that E3 solid samples presented a homogeneous morphology formed by particles mainly composed of As and Fe (point 2 of Fig. S6, supplementary material). Its composition and bipyramidal octahedral structure confirm that these particles are scorodite. The particle size was less than 10 μm, and aggregates were formed, in contrast to the results obtained for E1-B, where the particle size was around 20 μm and aggregates were not formed.

The major elements of the solid formed in experiment E4 (ES solution) are shown in Table 1. The E4 sample contained As (30.2±0.4%) and Fe (22.6±1.4%) as major elements and Cu (7.7±3.4%), Bi (2.7±0.5%), S (2.15±0.01%), and Sb (1.2±0.7%) in minor proportions. The XRD analysis is shown in Fig. S7 of the supplementary material, where it is observed that the solid did not present mineral phases, being formed by poorly crystalline ferric arsenate or amorphous ferric arsenate, similar to the obtained ones by other authors, such as ferric arsenate intermedium [$FeAsO_4 \cdot (2+x)H_2O$ $(0<x<1)$] (Le Berre et al., 2008; Min et al., 2015), ferric arsenate sub-hydrate or Phase 4 [$FeAsO_4 \cdot 3/4H_2O$], and basic ferric arsenate sulphate or Phase 3 [$Fe(AsO_4)_{1-x}(SO_4)_x(OH)_x(1-x)H_2O$ $(0<x<1)$] (Dutrizac and Jambor, 2007; Gomez et al., 2011b; Swash and Monhemius, 1998). The average experimental mass ratio of As/Fe was 1.33, which is similar to the theorical ratio of scorodite (As/Fe = 1.34), within the experimental uncertainties (≤ 10%). However, the loss on ignition (7.8±1.2%) was lower than the theoretical mass loss (about 15.5%) associated with the loss of the crystallisation water of $FeAsO_4 \cdot 2H_2O$.

On the other hand, the thermogravimetry analysis (Fig. S8 of the supplementary material) was performed to identify the compounds obtained in E4 according to its thermal behaviour. Four thermal events can be observed at 155 ºC, 506 ºC, 678 ºC, and 940 ºC. Water was only detected in the first event due to the loss of crystallised water of some hydrated compound. The second and third thermal events were due to the decomposition of sulphates, corroborated by the detection of SO_2 in the ICP-MS system. The thermal behaviour suggests that the compound obtained in E4 is analogous to the ferric arsenate sulphate or Phase 3 found by other authors (Dutrizac and Jambor, 2007; Gomez et al., 2011b) in which the decomposition occurs in three steps: (1) loss of crystallised water at 300–600 ºC; (2) sulphate decomposition at 650–820 ºC; and (3) arsenate decomposition at 820–975 ºC.

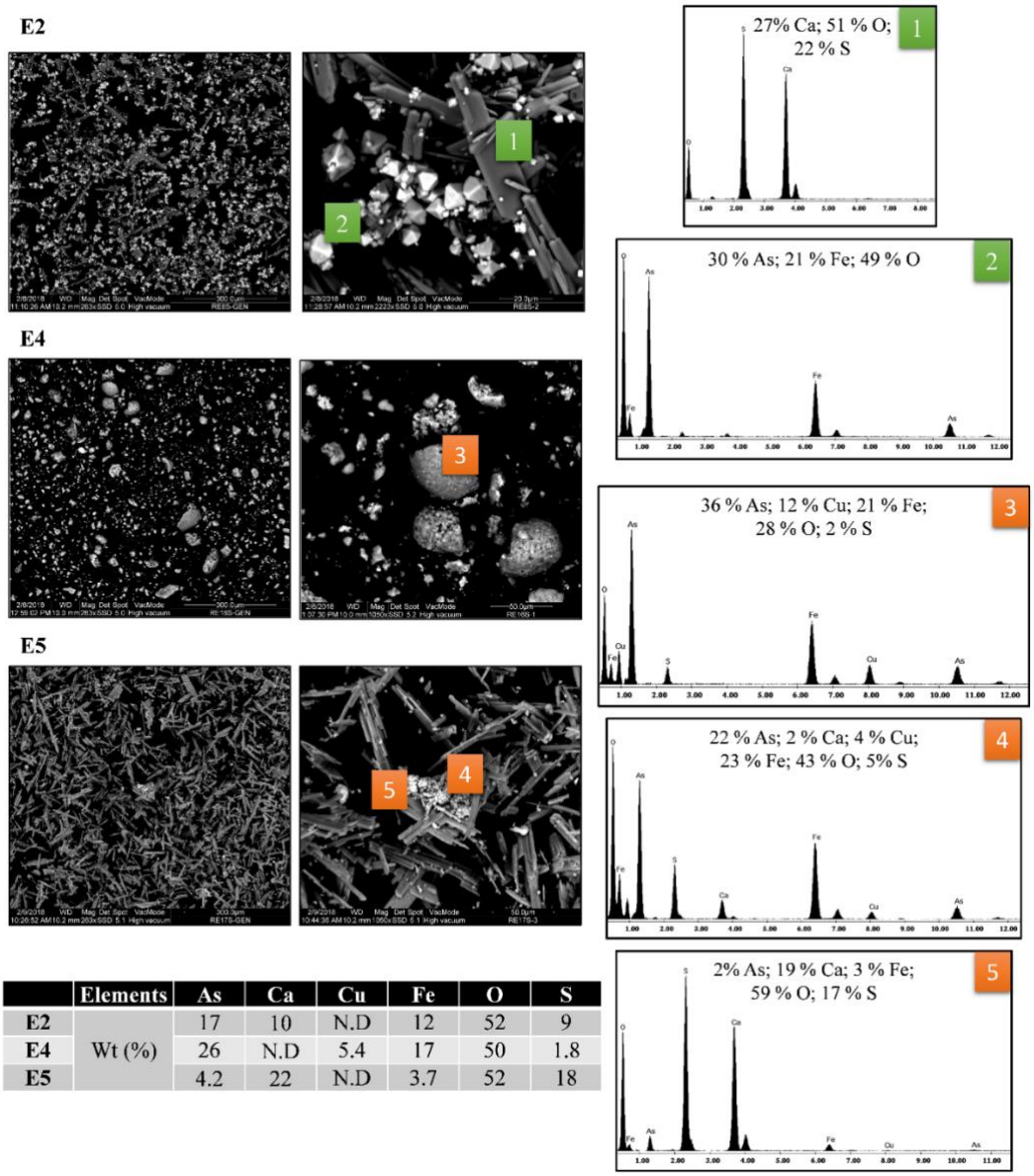

	Elements	As	Ca	Cu	Fe	O	S
E2	Wt (%)	17	10	N.D	12	52	9
E4		26	N.D	5.4	17	50	1.8
E5		4.2	22	N.D	3.7	52	18

Fig. 6. *SEM images of the precipitates obtained in experiments E2, E4, and E5. The table also shows the general composition determined by EDS from the image located at the left.*

The SEM analysis (Fig. 6) shows that the E4 solid presents an amorphous morphology composed of particle aggregates with sizes of 10–50 µm. These ones are mainly composed of As and Fe and Cu and S in minor proportions (point 3, Fig. 6). The obtained elemental composition of this sample by EDS agreed with the XRF results, which showed As, Fe, Cu, and S as the main elements.

The E5 sample is composed of As (10.9±1.2%), Ca (19.0±0.2%), Fe (10.3±0.1%), and S (15.4±0.5%) as main elements, whereas Cu, Sb, and Bi are present in proportion lower than 0.5%. The presence of Ca and S was expected when the neutralisation was carried out using $Ca(OH)_2$, as previously mentioned, due to gypsum formation (Bluteau et al., 2009; Demopoulos, 2005; Droppert, 1996). In fact, gypsum (≈ 83% $CaSO_4 \cdot 2H_2O$) was the only mineral phase identified in the E5 sample (Fig. S7 of the supplementary material), which is in agreement with the Ca and S concentrations provided by XRF, and this was confirmed by the mass ratio found (Ca/S = 1.23), which is analogous to the theoretical ratio of gypsum (Ca/S = 1.25). On the other hand, the E5 sample showed a high concentration of As and Fe. The experimental mass ratio (As/Fe = 1.05) found was lower than the theoretical ratio of scorodite (As/Fe = 1.34), and no evidence of its existence was found. Hence, the precipitated As and Fe probably form some type of ferric arsenate (≈ 17%), as mentioned for the E4 sample, such as ferric arsenate intermedium $[FeAsO_4 \cdot (2+x)H_2O]$, ferric arsenate sub-hydrate ($FeAsO_4 \cdot 3/4H_2O$), or basic ferric arsenate sulphate $[Fe(AsO_4)_{1-x}(SO_4)_x(OH)_x(1-x)H_2O]$ (Dutrizac and Jambor, 2007; Gomez et al., 2011b; Le Berre et al., 2008).

The SEM analysis of the E5 samples is shown in Fig. 6. The obtained elemental composition of these samples by EDS agrees with the results obtained by XRF, where the E5 matrix was mainly composed of As, Ca, Fe, and S. On the other hand, the solid presents a heterogenous morphology, and it is formed by two types of particles: (1) large particles composed of Ca and S, whose tabular structure correspond with gypsum (point 5 Fig. 6), verifying the results obtained by XRD, and (2) fine particles composed of As and Fe that do not have a crystalline structure, these form amorphous aggregates (point 4, Fig. 6) that are deposited on the gypsum surface.

In agreement with the consulted literature (Fujita et al., 2008b; Gomez et al., 2011a; Singhania et al., 2006), the formation of amorphous or poorly crystalline ferric arsenate in experiments E4 and E5 using the ES solution can be due to the incorporation of more than 5% SO_4 anions and cations (Cu^{2+}) into the crystal structure.

4. Practical implications

The removal of As, which is one of the impurities contained in Cu concentrate, has become one of the current challenges of the pyrometallurgical Cu industry since it negatively affects the Cu cathode. Part of the As that flows in the process is dissolved in the Cu electrolyte, and its concentration is reduced when it

is subjected to water treatment in which a solid is formed (ES), which is recirculated due to the high Cu content. The process proposed in this work focused on the separation of As and Cu through acid dissolution of the ES and subsequent precipitation of ferric arsenate, obtaining a final liquid effluent with free As and high Cu content. Therefore, the Cu could be returned in the process without impurities, and the ferric arsenate could be valorised by using it is in commercial applications such as the electrochemical energy storage in Li-battery (Anji Reddy et al., 2009; Gomez et al., 2013). In addition, the formation of scorodite is considered as an alternative for As stabilisation (Rong et al., 2020; Tabelin et al., 2019), keeping its stability under oxidising conditions in the pH range of 2.0–6.0 (KE and LIU, 2019; Riveros et al., 2001). The final wastewater stream, with a low concentration of As and Cu, could be sent to an effluent treatment plant (ETP) for final treatment before its release to the environment.

This procedure could be applied to other acidic liquid effluents that are generated during Cu cathode production; whose current treatment generates As-rich waste that is considered a hazardous material. Therefore, the procedure proposed in this work generates a dual benefit. On the one hand, from an environmental point of view, the decrease in the amount of produced waste and the reduction of the environmental impact due to potential liquid effluent releases, in our case of study into a very impacted environment as the Huelva estuary. On the other hand, from an economic point of view, part of the Cu is recovered, improving the industrial process yield. These facts approach the copper production industrial process to the aim of the circular economy.

5. Conclusions

The dissolution and subsequent treatment of highly Cu-rich ES with As impurities from the Cu production industry was developed in this work to decrease the As concentration and to recover the remaining Cu. The ES was fully dissolved (> 99%) in H_2SO_4/HNO_3 medium using a solid-to-liquid ratio of 1:20 for 2.5 h at 50 rpm. During treatment of the obtained solution, amorphous ferric arsenate was obtained, and the obtained PE for As was around 70%. In addition, around 50% Cu co-precipitated with the formed solid, suggesting that it would be more appropriate to perform previously Cu recovery as copper sulphate, which will also improve the subsequent PE of As. Therefore, more experiments to optimise the As removal process avoiding Cu co-precipitation, and study the inertisation process and/or the potential applications of the formed solid are required.

Acknowledgements

This research has been supported by the Atlantic Copper company project "Copper recovery and arsenic removal from electrolytic sludge generated in the electrolytic treatment plant", and the project of the Regional Government of Andalusia entitled "Basic processes regulating the fractionations and enrichments of natural radionuclides under acid mine drainage conditions" (Ref.: UHU-1255876).

References

Anji Reddy, M., Pralong, V., Caignaert, V., Varadaraju, U. V., Raveau, B., 2009. Monoclinic iron hydroxy sulphate: A new route to electrode materials. Electrochem. commun. 11, 1807–1810. https://doi.org/10.1016/j.elecom.2009.07.024

Artzer, A., Moats, M., Bender, J., 2018. Removal of Antimony and Bismuth from Copper Electrorefining Electrolyte: Part I—A Review. Jom 70, 2033–2040. https://doi.org/10.1007/s11837-018-3075-x

Atlantic Copper, 2017. Annual Environmental Report. Huelva, Spain.

Balaji, T., Yokoyama, T., Matsunaga, H., 2005. Adsorption and removal of As(V) and As(III) using Zr-loaded lysine diacetic acid chelating resin. Chemosphere 59, 1169–1174. https://doi.org/10.1016/j.chemosphere.2004.12.007

Bluteau, M.C., Becze, L., Demopoulos, G.P., 2009. The dissolution of scorodite in gypsum-saturated waters: Evidence of Ca-Fe-AsO4 mineral formation and its impact on arsenic retention. Hydrometallurgy 97, 221–227. https://doi.org/10.1016/j.hydromet.2009.03.009

Cao, Q., Chen, C., Li, K., Sun, T., Shen, Z., Jia, J., 2021. Arsenic(V) removal behavior of schwertmannite synthesized by KMnO4 rapid oxidation with high adsorption capacity and Fe utilization. Chemosphere 264, 128398. https://doi.org/10.1016/j.chemosphere.2020.128398

Cervando, L., Viraca, C., 2013. Termodinámica de la estabilización del arsénico. Rev. Met. UTO 34, 3–12.

Chen, M.L., Sun, Y., Huo, C.B., Liu, C., Wang, J.H., 2015. Akaganeite decorated graphene oxide composite for arsenic adsorption/removal and its proconcentration at ultra-trace level. Chemosphere 130, 52–58. https://doi.org/10.1016/j.chemosphere.2015.02.046

Cheng, R., Zhang, H., Ni, H., 2019. Arsenic removal from arsenopyrite-bearing iron ore and arsenic recovery from dust ash by roasting method. Processes 7. https://doi.org/10.3390/pr7100754

Dabekaussen, R., Droppert, D., Demopoulos, G.P., 2001. Ambient pressure hydrometallurgical conversion of arsenic trioxide to crystalline scorodite. CIM Bull. 94, 116–122.

Demopoulos, G.P., 2014. Arsenic immobilization research advances: past, present and future, in: Conference of Metallurgists Proceedings (COM). Canadian Institute of Mining, Metallurgy and Petroleum, Vancouver, Canada.

Demopoulos, G.P., 2005. On the preparation and stability of scorodite, in: Reddy, R.G., Ramachandran, V. (Eds.), Proceedings of Arsenic Metallurgy. The Minerals, Metals & Materials Society (TMS), Warrendale, PA., pp. 25–50.

Droppert, D.J., 1996. The ambient pressure precipitation of crytalline scorodite (FeAsO4 .2H2O) from sulphate solutions. McGill University Montreal, Canada.

Droppert, D.J., Demopoulos, G.., Harris, G.., 1996. Ambient pressure production of crystalline scorodite from arsenic-rich metallurgical effluent solutions, in: EPD Congress 1996, Warren, G.W. (Eds.), . The Minerals, Metals & Materials Society, 1996, pp. 227–239.

Dutrizac, J.E., Jambor, J.L., 2007. Characterization of the iron arsenate–sulphate compounds precipitated at elevated temperatures. Hydrometallurgy 86, 147–163. https://doi.org/10.1016/j.hydromet.2006.11.011

Fujita, T., Taguchi, R., Abumiya, M., Matsumoto, M., Shibata, E., Nakamura, T., 2009a. Effect of pH on atmospheric scorodite synthesis by oxidation of ferrous ions: Physical properties and stability of the scorodite. Hydrometallurgy 96, 189–198. https://doi.org/10.1016/j.hydromet.2008.10.003

Fujita, T., Taguchi, R., Abumiya, M., Matsumoto, M., Shibata, E., Nakamura, T., 2009b. Effect of pH on atmospheric scorodite synthesis by oxidation of ferrous ions: Physical properties and stability of the scorodite. Hydrometallurgy 96, 189–198. https://doi.org/10.1016/j.hydromet.2008.10.003

Fujita, T., Taguchi, R., Abumiya, M., Matsumoto, M., Shibata, E., Nakamura, T., 2008a. Novel atmospheric scorodite synthesis by oxidation of ferrous sulfate solution. Part II. Effect of temperature and air. Hydrometallurgy 90, 85–91. https://doi.org/10.1016/j.hydromet.2007.09.011

Fujita, T., Taguchi, R., Abumiya, M., Matsumoto, M., Shibata, E., Nakamura, T., 2008b. Effects of zinc,

copper and sodium ions on ferric arsenate precipitation in a novel atmospheric scorodite process. Hydrometallurgy 93, 30–38. https://doi.org/10.1016/j.hydromet.2008.02.016

Fujita, T., Taguchi, R., Abumiya, M., Matsumoto, M., Shibata, E., Nakamura, T., 2008c. Novel atmospheric scorodite synthesis by oxidation of ferrous sulfate solution. Part I. Hydrometallurgy 90, 92–102. https://doi.org/10.1016/j.hydromet.2007.09.012

Gomez, M.A., Becze, L., Celikin, M., Demopoulos, G.P., 2011a. The effect of copper on the precipitation of scorodite (FeAsO4·2H2O) under hydrothermal conditions: Evidence for a hydrated copper containing ferric arsenate sulfate-short lived intermediate. J. Colloid Interface Sci. 360, 508–518. https://doi.org/10.1016/j.jcis.2011.05.010

Gomez, M.A., Becze, L., Cutler, J.N., Demopoulos, G.P., 2011b. Hydrothermal reaction chemistry and characterization of ferric arsenate phases precipitated from Fe2(SO4)3-As 2O5-H2SO4 solutions. Hydrometallurgy 107, 74–90. https://doi.org/10.1016/j.hydromet.2011.01.007

Gomez, M.A., Ventruti, G., Celikin, M., Assaaoudi, H., Putz, H., Becze, L., Lee, K.E., Demopoulos, G.P., 2013. The nature of synthetic basic ferric arsenate sulfate (Fe(AsO 4)1-x(SO4)x(OH)x) and basic ferric sulfate (FeOHSO4): Their crystallographic, molecular and electronic structure with applications in the environment and energy. RSC Adv. 3, 16840–16849. https://doi.org/10.1039/c3ra42235f

Gonzalez-Contreras, P., Weijma, J., Van Der Weijden, R., Buisman, C.J.N., 2010. Biogenic scorodite crystallization by Acidianus sulfidivorans for arsenic removal. Environ. Sci. Technol. https://doi.org/10.1021/es902063t

Hao, L., Liu, M., Wang, N., Li, G., 2018. A critical review on arsenic removal from water using iron-based adsorbents. RSC Adv. https://doi.org/10.1039/c8ra08512a

ICSG, 2020. The World Copper Factbook 2020, International Copper Study Group (ICSC). Lisbon, Portugal.

Jain, C.K., Singh, R.D., 2012. Technological options for the removal of arsenic with special reference to South East Asia. J. Environ. Manage. 107, 1–18. https://doi.org/10.1016/j.jenvman.2012.04.016

KE, P. chao, LIU, Z. hong, 2019. Synthesis, in-situ coating and characterization of scorodite with high leaching stability. Trans. Nonferrous Met. Soc. China (English Ed. 29, 876–892. https://doi.org/10.1016/S1003-6326(19)64998-8

Khan, S.A.R., Yu, Z., Golpira, H., Sharif, A., Mardani, A., 2021. A state-of-the-art review and meta-analysis on sustainable supply chain management: Future research directions. J. Clean. Prod. 278, 123357. https://doi.org/10.1016/j.jclepro.2020.123357

Khan, S.A.R., Yu, Z., Sharif, A., Golpîra, H., 2020. Determinants of economic growth and environmental sustainability in South Asian Association for Regional Cooperation: evidence from panel ARDL. Environ. Sci. Pollut. Res. 27, 45675–45687. https://doi.org/10.1007/s11356-020-10410-1

Le Berre, J.F., Gauvin, R., Demopoulos, G.P., 2008. A study of the crystallization kinetics of scorodite via the transformation of poorly crystalline ferric arsenate in weakly acidic solution. Colloids Surfaces A Physicochem. Eng. Asp. 315, 117–129. https://doi.org/10.1016/j.colsurfa.2007.07.028

Le Berre, J.F., Gauvin, R., Demopoulos, G.P., 2007. Characterization of Poorly-Crystalline Ferric Arsenate Precipitated from Equimolar Fe(III)-As(V) Solutions in the pH Range 2 to 8. Metall. Mater. Trans. B 38, 751–762. https://doi.org/10.1007/s11663-007-9081-y

Lenoble, V., Chabroullet, C., Al Shukry, R., Serpaud, B., Deluchat, V., Bollinger, J.C., 2004. Dynamic arsenic removal on a MnO 2-loaded resin. J. Colloid Interface Sci. 280, 62–67. https://doi.org/10.1016/j.jcis.2004.07.034

Liao, M.I., Shih, X.H., Ma, H. wen, 2019. Secondary copper resource recycling and reuse: A waste input–output model. J. Clean. Prod. 239, 118142. https://doi.org/10.1016/j.jclepro.2019.118142

Litter, M.I., Morgada, M.E., Bundschuh, J., 2010. Possible treatments for arsenic removal in Latin American waters for human consumption. Environ. Pollut. 158, 1105–1118. https://doi.org/10.1016/j.envpol.2010.01.028

Min, X.B., Liao, Y.P., Chai, L.Y., Yang, Z.H., Xiong, S., Liu, L., Li, Q.Z., 2015. Removal and stabilization of arsenic from anode slime by forming crystal scorodite. Trans. Nonferrous Met. Soc. China (English Ed. 25, 1298–1306. https://doi.org/10.1016/S1003-6326(15)63728-1

Nidheesh, P. V., Singh, T.S.A., 2017. Arsenic removal by electrocoagulation process: Recent trends and removal mechanism. Chemosphere. https://doi.org/10.1016/j.chemosphere.2017.04.082

Riveros, P.A., Dutrizac, J.E., Spencer, P., 2001. Arsenic Disposal Practices in the Metallurgical Industry. Can. Metall. Q. 40, 395–420. https://doi.org/10.1179/cmq.2001.40.4.395

Rong, Z., Tang, X., Wu, L., Chen, X., Dang, W., Li, X., Huang, L., Wang, Y., 2020. The effect of precursor

speciation on the growth of scorodite in an atmospheric scorodite synthesis. R. Soc. Open Sci. 7. https://doi.org/10.1098/rsos.191619

Rosengrant, L., Fargo, L., 1990. Final Best Demonstrated Available Technology (BDTA) Background Document for K031, K084, K101, K102, Characterization As Wastes (D004), Characteristic Se Wastes (D010), and P and U Wastes Containing As and Se Listing Constituents.

Schwartz, D.M., Omaynikova, V.Y., Stocker, S.K., 2017. Environmental benefits of the CESL Process for the treatment of high-arsenic copper-gold concentrates, in: Hydroprocess-ICMSE. pp. 1–10.

Singhania, S., Wang, Q., Filippou, D., Demopoulos, G.P., 2006. Acidity, valency and third-ion effects on the precipitation of scorodite from mixed sulfate solutions under atmospheric-pressure conditions. Metall. Mater. Trans. B Process Metall. Mater. Process. Sci. 37, 189–197. https://doi.org/10.1007/BF02693148

Singhania, S., Wang, Q., Filippou, D., Demopoulos, G.P., 2005. Temperature and seeding effects on the precipitation of scorodite from sulfate solutions under atmospheric-pressure conditions. Metall. Mater. Trans. B Process Metall. Mater. Process. Sci. 36, 327–333. https://doi.org/10.1007/s11663-005-0062-8

Song, P., Yang, Z., Zeng, G., Yang, X., Xu, H., Wang, L., Xu, R., Xiong, W., Ahmad, K., 2017. Electrocoagulation treatment of arsenic in wastewaters: A comprehensive review. Chem. Eng. J. 317, 707–725. https://doi.org/10.1016/j.cej.2017.02.086

Swash, P.M., Monhemius, J., 1998. The Scorodite Process: a technology for the disposal of arsenic in the 21st century., Effluent Treatment in the Mining Industry. University of Concepción.

Tabelin, C.B., Corpuz, R.D., Igarashi, T., Villacorte-Tabelin, M., Ito, M., Hiroyoshi, N., 2019. Hematite-catalysed scorodite formation as a novel arsenic immobilisation strategy under ambient conditions. Chemosphere 233, 946–953. https://doi.org/10.1016/j.chemosphere.2019.06.020

Wesstrom, B.C., Araujo, O., 2012. Optimizing a cascading liberator. T.T. Chen Honor. Symp. Hydrometall. Electrometall. Mater. Charact. 01, 151–156. https://doi.org/10.1002/9781118364833.ch13

Zhang, T., Zhao, Y., Bai, H., Wang, W., Zhang, Q., 2019. Enhanced arsenic removal from water and easy handling of the precipitate sludge by using FeSO4 with CaCO3 to Ca(OH)2. Chemosphere 231, 134–139. https://doi.org/10.1016/j.chemosphere.2019.05.117

563 Zouboulis, A.I., Katsoyiannis, I.A., 2018. Recent advances in water and wastewater treatment with
564 emphasis in membrane treatment operations. Water (Switzerland).
565 https://doi.org/10.3390/w11010045
566